

Entropic and enthalpic effects in thin film blends of homopolymers and bottlebrush polymers

Adeline Huizhen Mah,^{†,‡,△} Travis Laws,^{¶,△} Wei Li,^{§,△} Hao Mei,^{||,⊥} Chance C. Brown,[§] Anton levlev,[§] Rajeev Kumar,^{*,§,#} Rafael Verduzco,^{*,||,@} and Gila E. Stein^{*,¶}

[†]*Materials Science and Engineering Program, University of Houston, Houston, TX 77204*

[‡]*Department of Chemical and Biomolecular Engineering, University of Houston, Houston, TX 77204*

[¶]*Department of Chemical and Biomolecular Engineering, University of Tennessee, Knoxville, TN 37996*

[§]*The Center for Nanophase Materials Sciences, Oak Ridge National Laboratory, Oak Ridge, TN 37831*

^{||}*Department of Chemical and Biomolecular Engineering, Rice University, Houston, TX 77005*

[⊥]*Department of Materials Science and NanoEngineering, Rice University, Houston, TX 77005*

[#]*Computational Chemical and Materials Sciences, Oak Ridge National Laboratory, Oak Ridge, TN 37831*

[@]*Materials Science and NanoEngineering, Rice University, Houston, TX 77005*

[△]*Equal contribution*

E-mail: kumarr@ornl.gov; rafaelv@rice.edu; gstein4@utk.edu

Abstract

We present a combined experimental and computational study of surface segregation in thin films of nearly-athermal blends of linear and bottlebrush polymers. The lengths of bottlebrush backbone (N_b), bottlebrush side chain (N_{sc}) and linear polystyrene host (N_m) are systematically varied to examine the effects of polymer architecture on phase behavior. From the experiments, combinations of architectural parameters are identified that produce enrichment and depletion of bottlebrush at the polymer-air interface. These surface segregation behaviors are consistent with entropy-dominated thermodynamics. In addition, the experiments reveal conditions where bottlebrush and linear polymers are equally preferred at the surface. Simulations based on the self-consistent field theory (SCFT) qualitatively capture the three types of surface segregation behaviors and highlight the delicate interplay of entropic and enthalpic effects. Our investigations demonstrate that controlling both entropic and enthalpic driving forces is critical for the design of surface-active bottlebrush polymer additives.

Introduction

Surface-active polymeric additives can decouple surface functions from bulk properties of the host polymer.¹⁻³ Enrichment of these additives near surfaces is driven by the reduction in surface free energy, so in a blend, the constituent with the lowest surface tension will spontaneously accumulate at the surface. For linear polymers, surface tension is dominated by enthalpic interactions prescribed by monomer chemistry, while entropic factors associated with molecular weight and chain stiffness play a secondary role. Therefore, in a blend of chemically-distinct linear polymers, the polymer with the lowest cohesive energy density is usually enriched at the surface.

When all constituents in a polymer blend have the same monomer chemistry (*i.e.*, an athermal system), the effects of chain length^{4,5} and architecture⁶⁻⁸ on surface tension become relevant. As examples, when linear polymers have a distribution of chain lengths, the shorter chains are attracted to the surface; and in a blend of branched and linear polymers, the branched polymer is usually attracted to a surface. These behaviors arise from an entropic preference for chain ends⁶⁻¹³ over “mid-monomers” at surfaces. In other words, long linear polymers, having a low ratio of chain ends to mid-monomers, experience a greater entropy loss at a surface compared with branched polymers or short linear polymers.^{8,14-16} An additional factor that controls surface attraction is the relative stiffness of each type of polymer. For instance, in the case of highly-branched bottlebrush polymers, steric interactions among side chains will produce an extended polymer backbone, effectively increasing the backbone Kuhn segment length.¹⁷ Such stiffening of the backbone causes entropic repulsion of bottlebrush polymers from a planar surface.¹⁸⁻²⁰

While bottlebrush polymers are widely studied for applications in drug delivery,^{21,22} photonics,^{23,24} lubricants,^{25,26} and responsive coatings,²⁷ there are few studies on surface attraction in blends of bottlebrush polymer additives and linear polymer hosts. Mayes and coworkers examined blends of chemically-distinct bottlebrush-like polymers and linear polymers, and showed that the strong entropic attraction of highly-grafted polymers to sur-

faces could overcome enthalpic preferences.^{8,28} A previous study from Stein, Verduzco, and coworkers examined the segregation behaviors in thin films containing blends of bottlebrush polystyrene and linear poly(d8-styrene) hosts.²⁹ The bottlebrush backbone and side-chain lengths were fixed while the host chain length was varied. Within the narrow parameter space considered, the bottlebrush was strongly preferred at surfaces when the host chains were much longer than bottlebrush side chains. Such behaviors were also captured in simulations of athermal linear/bottlebrush blends based on dissipative particle dynamics.³⁰ Collectively, these studies demonstrate that bottlebrush polymers can be engineered to spontaneously accumulate at the surface of a linear host. However, the observed behaviors in experiments are controlled by a combination of entropic effects and enthalpic interactions that arise from end-group chemistry,^{1,31,32} joint chemistry^{16,32} and isotopic labels.^{12,33} A concerted experimental and modeling effort is needed to efficiently explore a broader parameter space. Moreover, the modeling effort must account for entropic effects that are present at high grafting densities, as well as subtle enthalpic interactions that are difficult to avoid in experiments.

In this report, we investigate a broader parameter space than in our prior work²⁹ and systematically examine the effects of bottlebrush backbone length (N_b), bottlebrush side-chain length (N_{sc}), and linear host chain length (N_m) on as-cast and annealed thin films. These studies encompass an array of bottlebrush architectures ranging from star-like to cylindrical, with subtle differences in the chemistries of bottlebrush and linear polymers due to end-groups, joints and isotopic labels. The experimental studies reveal combinations of architectural parameters that produce enrichment and depletion of bottlebrush at the surface, and also show conditions of non-preferential wetting. Experimental results for the surface segregation of bottlebrush polymers are summarized in schematic phase diagrams in terms of two parameters, N_m/N_{sc} and N_b/N_{sc} , which describe the ratio of chain ends in bottlebrush and linear polymers and the architecture of bottlebrush polymers, respectively. We note that these results are partly controlled by system-specific parameters, such as the grafting density of bottlebrush side chains and the Kuhn lengths of each polymer, so the experimen-

tal schematic phase diagrams are not universally applicable. The experimental findings are corroborated by simulations based on the self-consistent field theory (SCFT), which successfully reproduced the three types of surface behaviors when weak polymer-surface interactions were included in the model. The qualitative agreement between experiments and simulations reveals a complex competition between entropic and enthalpic driving force that originates from the different architectures and chemistries of each constituent in the blend.

Experimental Section

Materials

Linear Polystyrene (PS) Homopolymers. PS standards were purchased from Scientific Polymers, Inc. Table 1 reports the PS specifications.

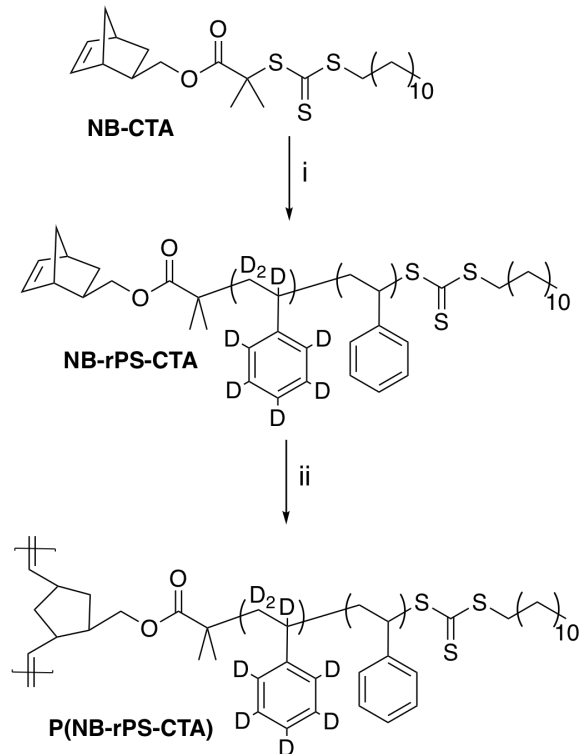
Table 1: Specifications of PS standards. M_n is number-average molecular weight, N_m is degree of polymerization, and \mathcal{D} is dispersity.

Polymer	M_n (kg/mol)	N_m	\mathcal{D}
PS2k	2.4	23	1.01
PS5k	4.8	46	1.05
PS8k	8.0	77	1.05
PS18k	18.0	173	1.01
PS32k	32.4	312	1.03
PS58k	58.0	558	1.01
PS87k	87.4	840	1.01
PS211k	211.5	2033	1.01

Reagents. Unless otherwise specified, all reagents and solvents were purchased from commercially available sources and used as received. Styrene was passed through an aluminum oxide column, and d8-styrene was distilled at 70 °C under vacuum to remove inhibitors. 2,2'-Azobis(2-methylpropionitrile) (AIBN) was purified by recrystallizing in methanol. Bicyclo[2.2.1]hept-5-en-2-ylmethyl 2-(((dodecylsulfanyl)(thioxo)methyl)sulfanyl)-

2-methylpropanoate (NB-CTA)³⁴ and the modified 2nd generation Grubbs ((H2IMes)(-pyr)2(Cl)2RuCHPh) catalyst³⁵ were synthesized according to methods in other reports.

Norbornene Functionalized Poly(d8-styrene-r-styrene) Macromonomer (NB-rPS-CTA). Linear poly(d8-styrene-r-styrene) macromonomers, NB-rPS-CTA, were prepared using reversible addition-fragmentation chain-transfer (RAFT) polymerization (Scheme 1). d8-styrene (d8S), styrene (S), NB-CTA, AIBN and toluene were added into a 10 mL round bottom flask equipped with a stir bar. The solution mixture was purged with nitrogen gas for 30 minutes and the polymerization was initiated by placing the flask in an oil bath at 70 °C. After 18 hours, the polymerization was quenched by immersing the flask in an ice bath. The polymer was then obtained by precipitating in methanol at 4°C and dried under vacuum. Three different molecular weights of rPS macromonomers were synthesized, ranging from 3 to 9 kg/mol. The molar ratios of each reagent used for the synthesis of the respective macromonomers are reported in Table S1.



Scheme 1: Synthetic scheme for the preparation of bottlebrush polymers with rPS-CTA side chains. i) RAFT (70 °C d8-styrene, styrene, AIBN, toluene). ii) ROMP, (CH₂Cl₂, (H₂IMes)(pyr)₂(Cl)₂RuCHPh).

Bottlebrush (BB) poly(d8-styrene-r-styrene). BB polymers with rPS-CTA side chains were prepared through the ring-opening polymerization (ROMP) of NB-rPS-CTA macromonomers using the modified 2nd generation Grubbs ((H₂IMes)(-pyr)₂(Cl)₂RuCHPh) catalyst (Scheme 1). In a representative example, a stock solution of the modified 2nd generation Grubbs catalyst was prepared in anhydrous DCM (1.09 mg, 0.0015 mmol, 0.003 M) in a 20 mL vial. In a separate 20 mL vial with a stir bar, NB-rPS-CTA ($N_{sc} = 28$, $M_n = 3.4$ kg/mol, 50 mg, 0.0147 mmol) was dissolved in anhydrous DCM (0.48 mL, 0.03 M solution). Next, 0.1 mL (0.0003 mmol) of the catalyst solution was added to initiate the reaction, and the reaction mixture was stirred at room temperature for at least 1 hr. The reaction was then quenched with 0.1 mL of butyl vinyl ether, and the product was recovered through precipitation in methanol at 4°C and drying under vacuum at room temperature. Based on the GPC analysis, all BB synthesized were

found to have a macromonomer conversion of >92%. ^1H NMR and GPC spectra for the bottlebrush polymers are provided in the Supporting Information Figures S1 and S2, respectively. The properties of the bottlebrush polymers used in this study are reported in Table 2.

Table 2: Properties of bottlebrush polymer additives with rPS-CTA side chains, where f_{d8S} denotes the molar fraction of d8-styrene in the side chains, N_{sc} is the average side-chain degree of polymerization, \mathbb{D}_{sc} is the side-chain molecular weight dispersity, N_b is the average backbone degree of polymerization, and \mathbb{D}_b is the molecular weight dispersity of the bottlebrush polymer. The calculation of N_{sc} neglects the CTA endgroup and only reflects the number of styrene and d8-styrene in the side chains.

Bottlebrush Polymer	f_{d8S}	N_{sc}	\mathbb{D}_{sc}	N_b	\mathbb{D}_b
NB ₂₄ S ₂₈	0.35	28	1.1	24	1.25
NB ₁₆₉ S ₂₈	0.35	28	1.1	169	2.34
NB ₂₂ S ₄₄	0.35	44	1.1	22	1.36
NB ₂₆ S ₇₇	0.42	77	1.1	26	1.52

Instrumentation

Gel Permeation Chromatography (GPC). Molecular weights and dispersities of rPS and BB polymers were obtained using an Agilent 1200 module containing three PSS SDV columns in series (100, 1000 and 10000 Å pore sizes), an Agilent variable wavelength UV/vis detector, a Wyatt Technology HELEOS II multiangle laser light scattering (MALLS) detector ($\lambda = 658\text{nm}$), and a Wyatt Technology Optilab rEX RI detector. This system enables size exclusion chromatography (SEC) with simultaneous refractive index (SEC-RI), UV/vis (SEC-UV/vis) and MALLS detection. THF was used as the mobile phase with a flow rate of 1 mL/min at 40°C. The conversions of the synthesized bottlebrush polymers were determined by comparing the peak areas of the rPS BB polymers and unreacted rPS macromonomers. The refractive index (dn/dc) of each rPS BB polymers was calculated with the assumption of 100% mass recovery and corrected by using the actual injected mass of BB in the solution. This correction accounts for the unreacted rPS macromonomers after the ROMP reaction.

Nuclear Magnetic Resonance Spectroscopy (NMR). Using a 400 MHz Bruker multinuclear spectrometer, the hydrogen NMR (^1H NMR) spectra were obtained in CDCl_3 with tetramethylsilane as an internal standard. Samples were prepared with a concentration of 10 mg/mL in 5 mm o.d. tubes.

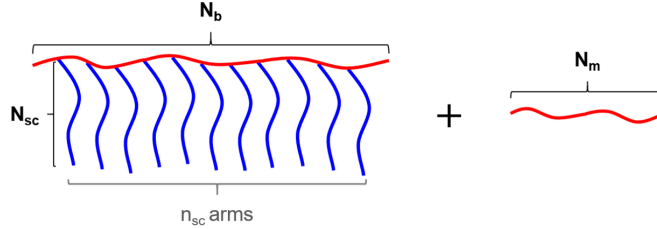
Spectroscopic Ellipsometry. The thicknesses of the polymer films were measured using a J.A. Woollam M-2000 spectroscopic ellipsometer. The ellipsometry parameters Δ and Ψ were modeled by describing the polymer’s optical properties with the Cauchy dispersion relation, $n(\lambda) = A + B/\lambda^2$, where λ is the incident wavelength (nm). The Cauchy constants (A, B) and film thickness were adjustable parameters for regression analysis. Typical values of the A and B parameters are 1.5 and 0.01, respectively.

Time of Flight Secondary Ion Mass Spectrometry (TOF-SIMS). The depth-dependent composition of each thin film blend was measured using a ToF-SIMS V (ION-TOF GmbH, Germany) instrument at Oak Ridge National Laboratory. Measurements were performed using a Bi/Mn liquid metal ion gun (LMIG) and an argon gas cluster ion gun that were operated in non-interlaced, dual beam mode with alternating sputtering and analysis cycles. For all samples, the Ar_n^+ (5 keV, 4 nA, $n = 1500$ or 10 keV, 10 nA, $n = 2300$) beam was rastered over a $500 \mu\text{m}^2$ area with a central Bi_3^+ (30 keV, 45 nA, high spectral resolution mode) analysis beam region of $200 \mu\text{m}^2$. An electron flood gun was used for charge compensation operating at 21 eV and $20 \mu\text{A}$. Positive secondary ions were collected at a rate of 2 frames/sec to maximize signal to noise. The spectral resolution of the ToF mass analyzer was < 0.0005 Da. For this study, we used the deuterium secondary ion counts ($^2\text{H}^+$) to track the distribution of bottlebrush polymers throughout the film thickness, and we used positive silicon secondary ions (Si_2^+) to detect the polymer/substrate interface. Procedures for calibrating the sputtering rate and the ion signal are provided in the Supporting Information. An example of sputter rate calibration is shown in Figures S3-S4, and the calibration curve for the $^2\text{H}^+/\text{C}^+$ ion ratio is reported in Figure S5.

Thin Film of Polymer Blends. Linear PS and BB polymers were dissolved in chlorobenzene at a 9:1 ratio (wt/wt). The concentration of the solids varied from 5.5-6.5 wt%. The films were prepared using a flow coater which was built following a reported design.³⁶ The gap height used for coating was approximately 500 μm , and the blade was a 3 inch \times 1 inch glass microscope slide. 50 μL of polymer solution was flow coated onto clean (100)-oriented p-type 4 inch diameter silicon wafers. The velocity used for coating was adjusted from sample-to-sample to generate a film thickness of (300 ± 30) nm. The samples were then cut down to 1.2 cm \times 1.2 cm size. Some pieces were set aside to measure the structure that forms during solution casting. Other pieces were annealed at 150°C for 3 days in a nitrogen-purged glove box (3 ppm O₂, < 1 ppm moisture).

Simulation Model and Method

We used a field-theoretic model to examine segregation near surfaces in thin films containing almost athermal binary polymer blends. To study the effects of chain architecture on the surface segregation, we picked a model system of AB multi-graft/comb copolymers and A linear homopolymers (Scheme 2). Specifically, the comb copolymers had a backbone with N_b Kuhn statistical segments of monomer A. The backbone was grafted with n_{sc} linear side chains of monomer B, producing a side-chain grafting density of n_{sc}/N_b . Each side chain had N_{sc} segments of monomer B. The total degree of polymerization of the comb copolymer was then $n_{sc}N_{sc} + N_b$. The linear homopolymer was defined with N_m segments of monomer A. AB comb copolymers were chosen to represent the bottlebrush polymers, because this model can capture the different side chain and homopolymer chemistries in experiments.



Scheme 2: Illustration of comb copolymer and homopolymer architectures studied in this work.

Both the comb copolymers and the linear polymers were modeled as continuous Gaussian chains. We note that using Gaussian chains to represent the backbones of norbornene-based bottlebrushes is a simple choice that was used in other field-theoretic models of bottlebrush polymers.³⁷ Alternatively, a wormlike chain model for the semiflexible backbone can be adopted.³⁸ Our choice of the Gaussian-chain model was motivated by the fact that entropic effects resulting from the different rigidities of bottlebrush backbones and homopolymers can be mimicked by varying the conformational asymmetry of the respective Kuhn segments.¹⁷ Therefore, the model based on Gaussian chains is sufficient to understand the surface segregation of bottlebrush polymers.

Interactions between A and B segments were modeled using a Flory-Huggins interaction parameter $\chi = 1.7 \times 10^{-4}$, which is the reported interaction parameter between PS and dPS.³⁹ Thin films were simulated by including walls in the model, which were numerically implemented by the masking method^{40,41} with prescribed wall density profiles. The interactions between the walls and polymers were also depicted by Flory-Huggins parameters, which qualitatively captured the wetting conditions at the polymer-air and polymer-substrate interfaces. A general recipe for statistical field theory of the model can be found elsewhere.^{20,41,42} Standard saddle-point approximation was invoked and the modified diffusion equations were solved *via* a pseudo-spectral algorithm.⁴² The simulations were performed using PolySwift++.⁴³

Results and Discussion

Blends of linear PS and bottlebrush rPS were prepared with a 9:1 (wt/wt) ratio in chlorobenzene. We assume that the densities of linear PS and bottlebrush rPS are the same, so volume fraction and weight fraction are equivalent. Films with thicknesses of 350 ± 20 nm were prepared by flow coating onto clean silicon (Si) wafers and annealed at 150 °C for 3 days. The film surfaces (as-cast and annealed) were imaged with atomic force microscopy and optical microscopy, and there are no signs of lateral phase separation in these images (see Figures S6-S9). The depth-dependent composition of bottlebrush polymer was measured with TOF-SIMS. The $^2\text{H}^+$ signal is unique to rPS side chains was used to calculate the rPS volume fraction (ϕ) as a function of depth into the film. This approach does not distinguish between the bottlebrush side chains and un-reacted macromonomer. However, the un-reacted macromonomer comprised less than 0.8% of the total blend, and the effects of architecture on surface attraction are much stronger than the effects of chain length in these blends.

Figure 1 reports the as-cast depth profiles for films with $\text{NB}_{24}\text{S}_{28}$, $\text{NB}_{22}\text{S}_{44}$ and $\text{NB}_{26}\text{S}_{77}$ additives as a function of the linear PS chain length (N_m). The position of the polymer-air interface is defined as depth = 0 nm, and the position of the polymer-Si interface is marked by the red vertical line. All blends contain 10% bottlebrush additive, so if the bottlebrush polymers are uniformly distributed throughout the film, then the volume fraction of rPS side chains should be $\phi = 0.1$ at all depths. When the lengths of linear PS chains and bottlebrush rPS side chains are similar (*i.e.*, $N_m/N_{sc} \sim 1$), there is a slight enrichment of bottlebrush additive near the polymer-Si interface, but the composition is otherwise constant with depth at $\phi \approx 0.1$. As the length of the linear PS chain is increased ($N_m/N_{sc} \sim 7 - 20$), the bottlebrush is enriched at the surface of all films. Notably, the strong enrichment at depth = 0 nm demonstrates that top of the film has a nearly-pure layer of bottlebrush polymer (*i.e.*, $\phi \rightarrow 1$).

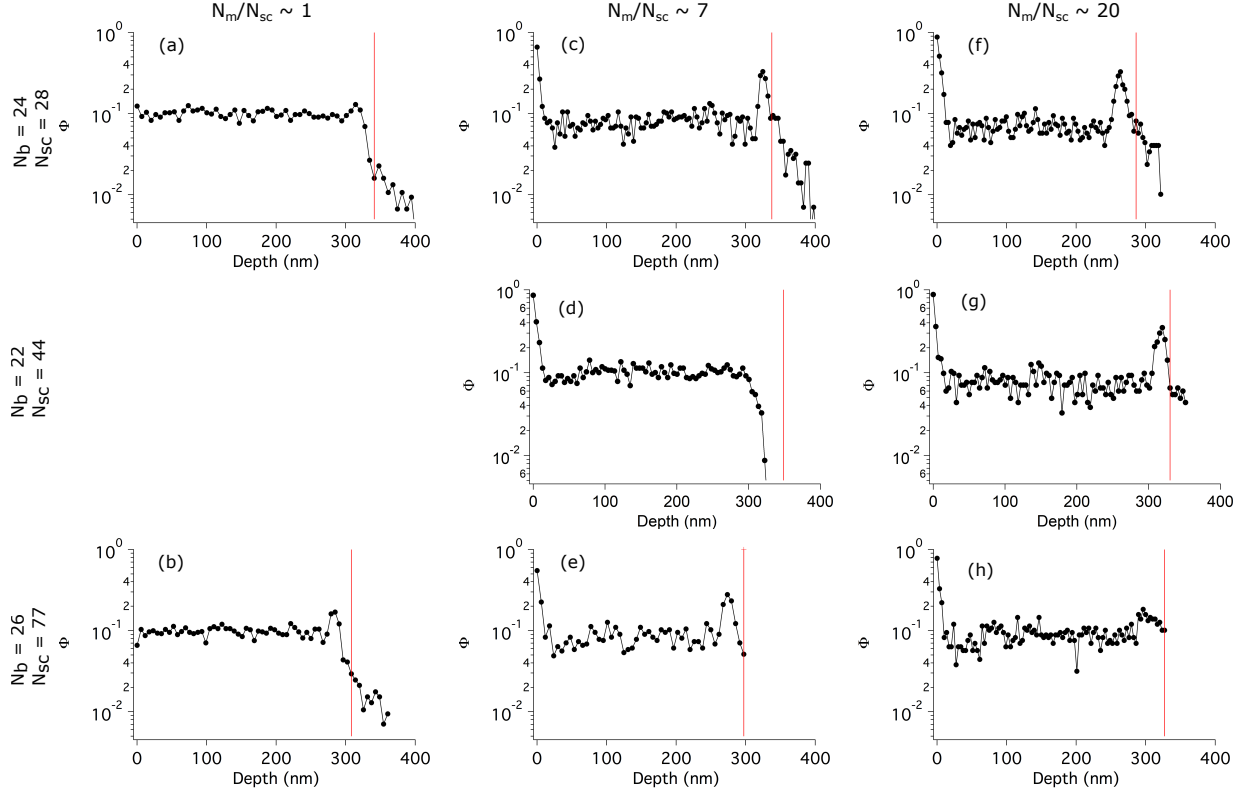


Figure 1: Volume fraction (ϕ) of rPS side chains as a function of depth in as-cast films. The position of the polymer-air interface is at depth = 0 nm, and the position of the polymer-Si interface is marked by the red vertical line. The bottlebrush side-chain length (N_{sc}) and backbone length (N_b) are fixed in each row. The ratio of linear PS chain length to bottlebrush rPS side-chain length (N_m/N_{sc}) is fixed in each column.

We also consider the effects of processing on the as-cast film structures. Specifically, we prepared thin film blends of NB₂₂S₄₄ with linear PS ($N_m/N_{sc} \sim 20$) were prepared by flow coating and spin coating from both chlorobenzene and toluene. The drying time was longest for flow coating from chlorobenzene and shortest for spin coating from toluene. Both coating methods produce a directional drying process that starts at the free surface. The depth-dependent bottlebrush composition for each combination of solvent and coating method is reported in Figure S10. We observe two trends in the data. First, the flow-coated samples exhibit a larger surface composition of bottlebrush (by approximately 20%) compared to the spin casted samples, and this behavior is independent of the solvent used. Second, samples cast from chlorobenzene have a larger surface composition of bottlebrush (by approximately

15%) than samples cast from toluene. A similar dependence of film morphology on solvent evaporation rate is observed in other polymer blend systems and was recently described using principles of linear non-equilibrium thermodynamics.⁴⁴

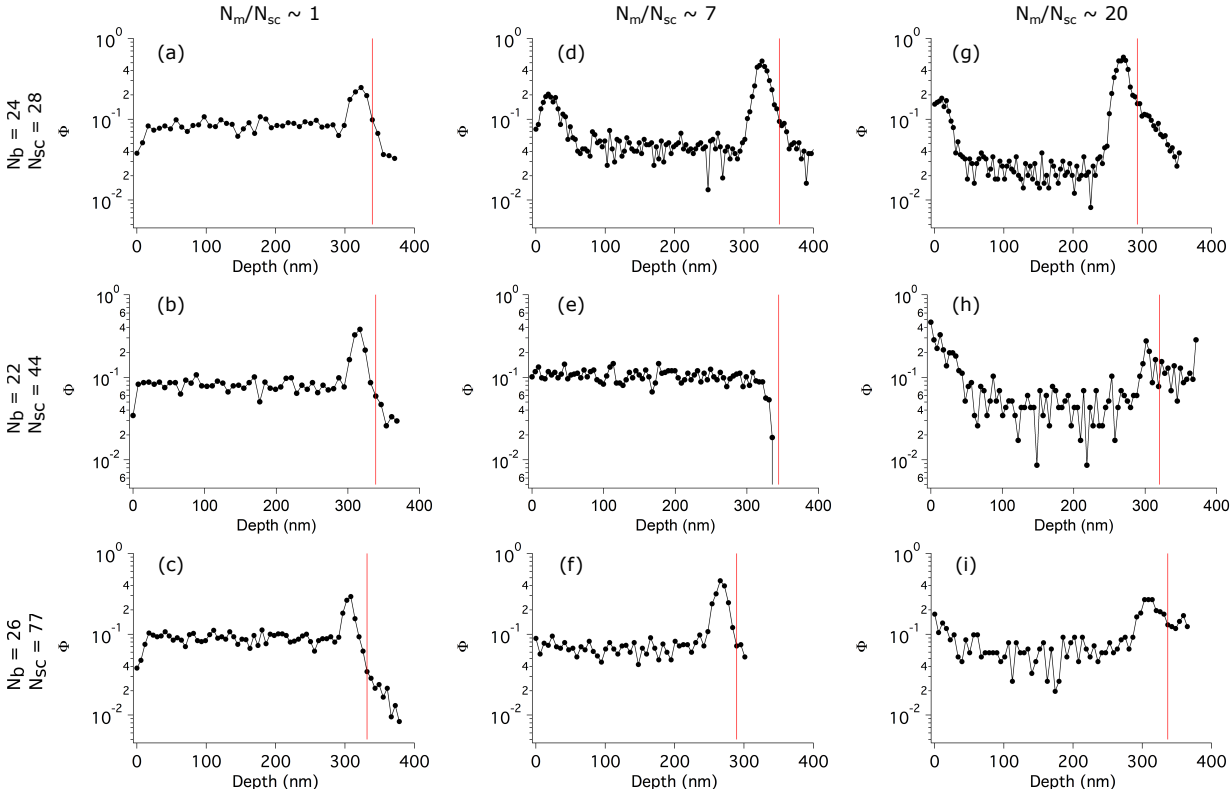


Figure 2: Volume fraction (ϕ) of rPS side chains as a function of depth in annealed films (150 °C). The position of the polymer-air interface is at depth = 0 nm, and the position of the polymer-Si interface is marked by the red vertical line. The bottlebrush side-chain length (N_{sc}) and backbone length (N_b) are fixed in each row. The ratio of linear PS chain length to bottlebrush rPS side-chain length (N_m/N_{sc}) is fixed in each column.

Figure 2 reports the depth profiles for films containing $NB_{24}S_{28}$, $NB_{22}S_{44}$ and $NB_{26}S_{77}$ additives after annealing at 150°C for 3 days. Compared with as-cast films, the depth profiles of annealed films show an enhanced bottlebrush composition ($\phi > 0.1$) at the polymer-Si interface for nearly all samples. Moreover, the depth profiles of annealed films reveal three types of behavior at the polymer-air interface: depletion of bottlebrush ($\phi < 0.1$), enrichment of bottlebrush ($\phi > 0.1$), and neither depletion nor enrichment of bottlebrush ($\phi \approx 0.1$). When $N_m/N_{sc} \sim 1$, all three types of bottlebrush additive are depleted from the polymer-air

interface, which means the short linear polymers are preferred at the polymer-air interface. When $N_m/N_{sc} = 7$, the $NB_{24}S_{28}$ additive is enriched near the polymer-air interface. However, while the as-cast films with $NB_{24}S_{28}$ have the maximum bottlebrush composition at depth = 0 nm, the annealed films show the maximum deeper into the film. In an athermal system, this behavior can be attributed to competing entropic forces: the surface will attract chain ends but also repel the backbone joints.¹⁴ A weak enthalpic attraction between the linear polymer and free surface could also contribute to this effect. In contrast to films with $NB_{24}S_{28}$, the depth profiles for films with $NB_{22}S_{44}$ and $NB_{26}S_{77}$ show neither depletion nor enrichment of bottlebrush at the polymer-air interface. When $N_m/N_{sc} = 20$, the depth profiles for all films show enrichment of the bottlebrush near the polymer-air interface, although this effect is very weak for $NB_{26}S_{77}$.

The effects of backbone length on surface composition are revealed by comparing the depth profiles for $NB_{24}S_{28}$ and $NB_{169}S_{28}$ bottlebrush additives with $N_m/N_{sc} \sim 7$. These two bottlebrush polymers have the same side-chain lengths ($N_{sc} = 28$) but different backbone lengths ($N_b = 24$ and 169). The results for $NB_{24}S_{28}$ are shown in Figure 1c (as-cast) and Figure 2d (annealed), and those for $NB_{169}S_{28}$ are provided in Figure S11 (as-cast and annealed). Both additives accumulate near the polymer-air interface after casting. However, after annealing, the maximum surface composition of $NB_{169}S_{28}$ is greater than that of $NB_{24}S_{28}$, with values of $\phi = 0.53$ and 0.21, respectively. This observation demonstrates that chain-end attraction dominates over joint/backbone repulsion, as noted in other studies that examined surface attraction of branched polymers using linear response theory.^{6,16} In addition, the maximum bottlebrush composition is moved slightly deeper into the film with $NB_{169}S_{28}$ (at depth = 23 nm) compared to $NB_{24}S_{28}$ (at depth = 18 nm), which demonstrates that surface repulsion increases with the number of backbone joints.¹⁴

We summarize the observed surface segregation behaviors for as-cast and annealed samples in Figure 3a and 3b, respectively. In addition to the data from this study (closed symbols), we also incorporate data from our previous study²⁹ (open symbols) to generate

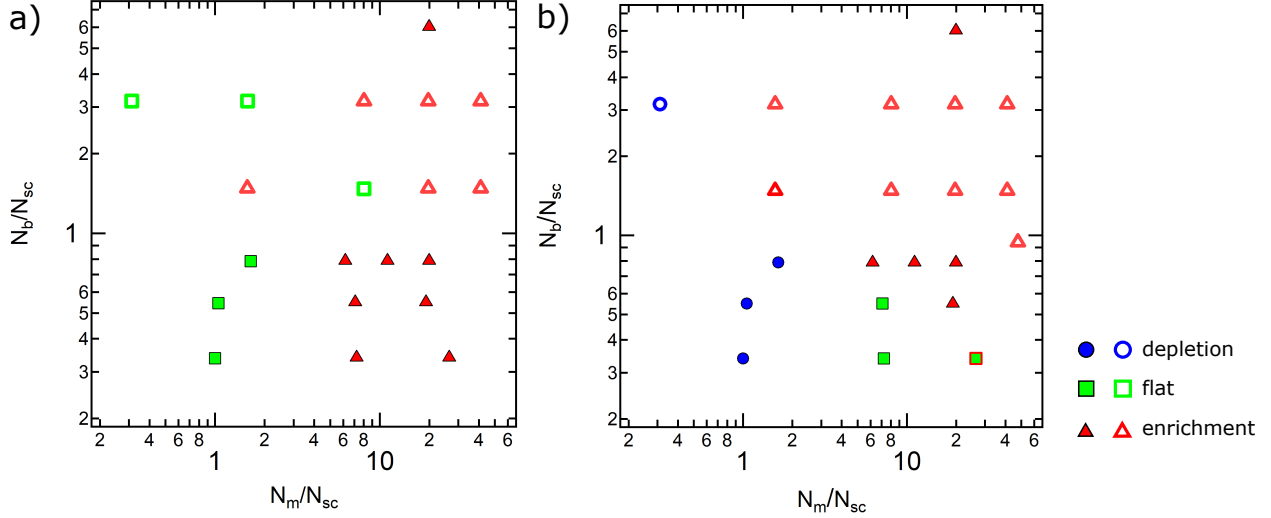


Figure 3: Summary of segregation behaviors near the polymer-air interface in blends of bottlebrush (10%) and linear (90%) polystyrene. (a) As-cast and (b) Annealed at 150°C for 3 days (closed symbols) or 7 days (open symbols). Depth profiles that show surface enrichment of bottlebrush = red triangles; depth profiles that show surface depletion of bottlebrush = blue circles; and depth profiles that appear “flat” = green squares.

a more comprehensive summary (while neglecting a few minor differences between these investigations). We report outcomes as a function of N_b/N_{sc} and N_m/N_{sc} rather than constructing a three-dimensional diagram to summarize the independent variation of N_b , N_{sc} and N_m . It is readily shown that N_b/N_{sc} and N_m/N_{sc} control the entropic contributions to the bulk phase behavior, along with the grafting density and the conformational asymmetry parameter (see Supporting Information Section 5 for details). The ratio N_b/N_{sc} qualitatively describes the aspect ratio of bottlebrush polymers. The ratio N_m/N_{sc} quantifies the relative fraction of chain ends in bottlebrush and linear polymers, which is given by $\eta = \left(\frac{n_{sc}}{n_{sc}N_{sc}+N_b}\right) / \left(\frac{2}{N_m}\right) = \frac{N_m}{2N_{sc}} \left(1 + \frac{N_b}{n_{sc}N_{sc}}\right)^{-1} \approx N_m/(2N_{sc})$, where the latter equality is obtained by assuming $n_{sc}N_{sc} \gg N_b$. We note that some of the bottlebrush polymers have broad dispersities in the backbone molecular weight, so each data point in Figure 3 reflects the average behavior for a range of bottlebrush polymers with different backbone lengths. While backbone dispersity can influence the location of the phase boundaries, this effect does not impact the general trends.

Figure 3a summarizes the key characteristics of depth profiles in as-cast films, and demonstrates that the parameter N_m/N_{sc} fully describes the transition between two types of surface behaviors: When $N_m/N_{sc} < 4$, the depth profiles are generally “flat” ($\phi \approx 0.1$), meaning there is neither depletion nor enrichment of bottlebrush at the polymer-air interface. When $N_m/N_{sc} > 4$, the depth profiles show an enrichment of bottlebrush at the polymer-air interface ($\phi > 0.1$). The surface enrichment is attributable to kinetic effects during film casting and drying process: specifically, the different mobilities of bottlebrush and linear polymers can give rise to a “skin” layer with a composition that strongly depends on the solvent evaporation rate.^{44,45} Understanding the kinetics that control the as-cast surface composition is beyond the scope of this work. However, it is interesting to note that simple processing approaches can produce a large bottlebrush composition at the film surface.

In Figure 3b, we summarize the three observed behaviors at the polymer-air interface for annealed films: depletion of bottlebrush, enrichment of bottlebrush, and neither depletion nor enrichment of bottlebrush (“flat” depth profiles). Depletion of bottlebrush is observed when the linear host chains have similar lengths as the bottlebrush side chains, which means the surface attraction of bottlebrush is weakened due to relatively fewer chain ends (*i.e.*, reduced η). Enrichment of bottlebrush is observed when N_m/N_{sc} and N_b/N_{sc} are both large. Surfaces with neither depletion nor enrichment of bottlebrush are observed when N_b/N_{sc} is small and N_m/N_{sc} is large. Overall, the diagrams in Figure 3a-b represent a simple and intuitive way to summarize the key characteristics of depth profiles, and suggest that the ratios N_m/N_{sc} and N_b/N_{sc} are useful parameters for characterizing the surface segregation behaviors in blends of bottlebrush and linear polymer.

To further explore the interface-induced segregation, as well as to understand the results presented in Figure 3b, we implemented SCFT calculations on blends of linear homopolymers and comb copolymers (see Scheme 2). We began the investigation with neutral confining walls that have no enthalpic interactions with either type of monomer. We examined a series of comb copolymers that have the same backbone length ($N_b = 20$) and grafting density

($n_{sc}/N_b = 0.5$) but different values of N_{sc} . The grafting density of one side chain for every two backbone Kuhn segments is similar to the grafting density of bottlebrush polymers in experiments (one side chain per five backbone carbons). The total volume fraction of comb copolymer in the blends was fixed at 10% to match the experiments.

Figure 4 reports the side-chain composition (ϕ) as a function of distance from a polymer-wall interface; the other boundary is omitted because the depth profiles are symmetric with neutral confinement. N_{sc} is fixed in each panel while N_m is varied. To compare with the experimental results, we arbitrarily define that a depth profile is “flat” when its maximum surface composition is within 5% of the composition in the middle of the film. (Figure S13 compares three SCFT depth profiles that show depletion of bottlebrush, a “flat” composition, and enrichment of bottlebrush.) For each value of N_{sc} , the depth profiles show a transition in bottlebrush surface composition from depletion (purple) to “flat” (cyan) to enrichment (all others) with increasing N_m/N_{sc} . When $N_m/N_{sc} = 1$, the comb polymer side chains are depleted from the non-selective boundary, which means the linear homopolymer is enriched at the interface. As N_m/N_{sc} increases, the comb polymer side chains are enriched at the non-selective boundary. This transition is explained by a simple analysis of the number of chain ends relative to mid-monomers in each polymer architecture, as the end segments suffer a lesser entropy loss near a surface compared with other segments. As previously discussed, the parameter $\eta \approx N_m/(2N_{sc})$ captures the relative chain end fractions for comb and linear polymers. When $\eta > 1$ ($N_m/N_{sc} > 2$), the entropic surface attraction of comb copolymers is stronger than that of linear homopolymers, producing an enrichment of comb copolymer near the boundary. Moreover, the change in surface enrichment with increasing N_m/N_{sc} is more pronounced with longer side chains (larger N_{sc}), which is attributed to increased segregation strength and reduced mixing entropy (see Section 5 in the Supporting Information).

Comparing the neutral wall case in Figure 4 with the experimental results, one finds two significant discrepancies. First, when $N_m/N_{sc} \approx 1$, the experiments (Figure 2a-c) show accumulation of bottlebrush at the substrate while the model predicts depletion. This implies

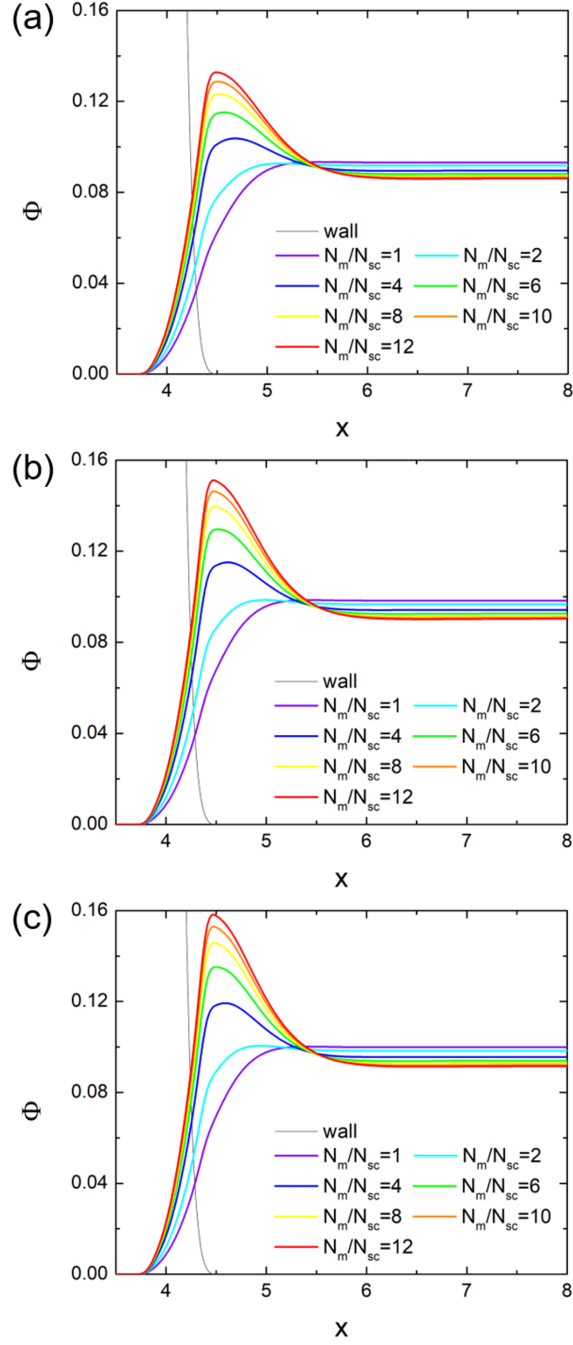


Figure 4: Volume fraction of side chains (ϕ) near a non-selective wall. Blends containing linear homopolymers (90 vol%) and 10-arm comb copolymers (10 vol%) were simulated for $n_{sc}=10$, $N_b = 20$, and film thickness (*i.e.*, wall separation) $h = 25.6$. (a) $N_{sc} = 20$, (b) $N_{sc} = 40$, and (c) $N_{sc} = 60$. All distances are presented in units of radius of gyration of the comb copolymer.

that the substrate has preferential interactions with the bottlebrush rPS polymer. To capture this effect, the model must include either attractive side-chain/substrate interactions or repulsive homopolymer/substrate interactions. Second, when $N_m/N_{sc} = 7$ and 20, the experiments (Figure 2d-i) show that increasing N_{sc} will reduce the amount of bottlebrush at the polymer-air interface, but the model predicts the opposite trend. This implies an enthalpic preference for the linear PS homopolymer at the polymer-air interface. Therefore, to improve agreement with experiments, we include selective interactions between the linear homopolymer and each wall in the SCFT model. We use $\chi_{twh} = -0.03$ and $\chi_{bwh} = 0.05$ to describe the interactions of homopolymers at the polymer-air and polymer-substrate interfaces, respectively. As shown in Figure 5, the SCFT depth profiles show qualitative agreement with experimental findings, demonstrating that the segregation behaviors at each boundary are controlled by a combination of entropic and enthalpic effects.

Next, we examined the surface segregation behavior with varying χ_{twh} . The results are summarized in schematic phase diagrams as shown in Figure 6. At $\chi_{twh} = 0$ (*i.e.*, neutral polymer-air interface), the surface segregation behavior is primarily controlled by N_m/N_{sc} . When $N_m/N_{sc} = 1$, the depth profiles show depletion of comb copolymer from the surface. When $N_m/N_{sc} = 2$, “flat” depth profiles are observed, which means the comb copolymer and linear homopolymer are equally attracted to the surface. When $N_m/N_{sc} \geq 4$, the depth profiles show enrichment of bottlebrush near the surface. As the magnitude of χ_{twh} increases, the homopolymers are more strongly attracted to the surface, and the area of the phase diagram corresponding to surface enrichment of comb copolymers is reduced. Similar trends are observed when the number of side chains is doubled to $n_{sc} = 20$, as shown in Figure S18.

The schematic phase diagrams based on the SCFT calculations with homopolymer/wall interactions show qualitative agreement with experiments (Figure 3b). However, it is unclear why the homopolymer is enthalpically favored over bottlebrush polymer at the air interface. Prior studies have shown that deuteration will reduce the surface tension of linear

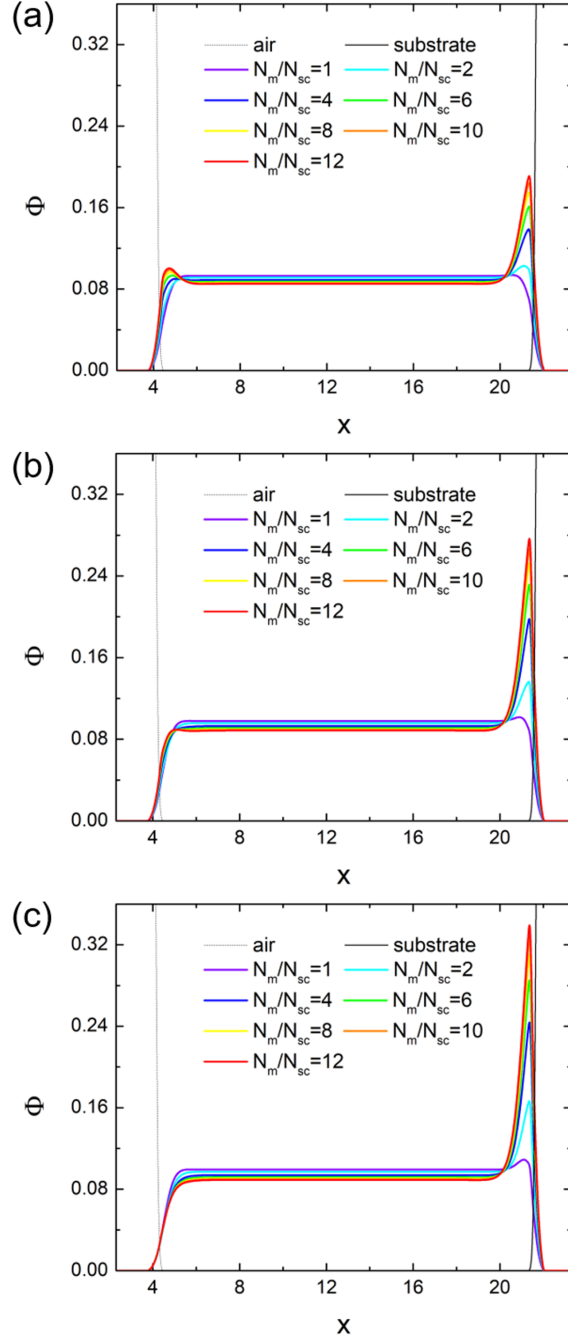


Figure 5: Volume fraction of side chains (ϕ) through the film thickness with asymmetric wetting at the boundaries. Blends containing linear homopolymers (90 vol%) and 10-arm comb copolymers (10 vol%) were simulated for $n_{sc}=10$, $N_b = 20$, $h = 25.6$, $\chi_{twh} = -0.03$ (air) and $\chi_{bwh} = 0.05$ (substrate). (a) $N_{sc} = 20$, (b) $N_{sc} = 40$, and (c) $N_{sc} = 60$. All distances are reported in units of radius of gyration of the comb copolymer.

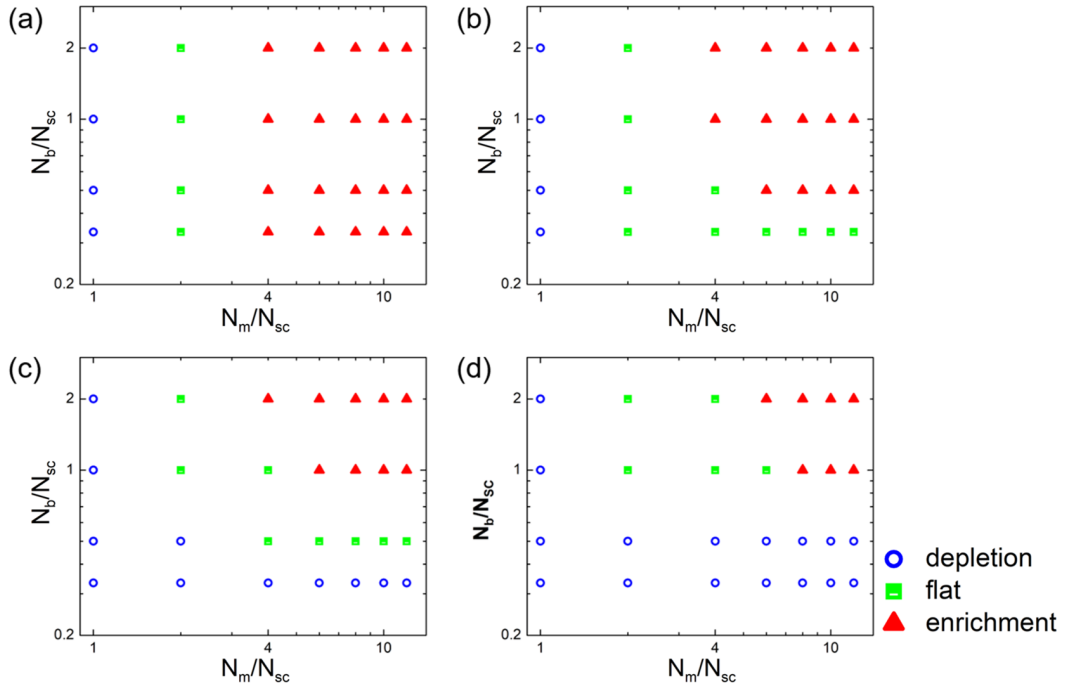


Figure 6: Schematic phase diagrams based on SCFT calculations of confined comb copolymer/linear homopolymer blends (10/90 vol/vol) for $N_b = 20$, $n_{sc} = 10$, and $h = 25.6$, with selective wetting at the boundaries: (a) $\chi_{twh} = 0$, (b) $\chi_{twh} = -0.02$, (c) $\chi_{twh} = -0.03$, and (d) $\chi_{twh} = -0.04$ at the free surface, while $\chi_{bwh} = 0.05$ at the substrate. See Figures S14-17 for corresponding depth profiles.

PS (assuming constant molecular weight),³³ so the bottlebrush rPS side chains should be enthalpically preferred over linear PS at the polymer-air interface. The bottlebrush has a norbornyl backbone and dodecyl trithiocarbonate end groups (Scheme 1), and these chemistries will introduce new types of interactions at surfaces and interfaces.⁴⁶ To test for an enthalpic preference of linear PS over the bottlebrush side chains at the free surface, we performed control experiments using blends of NB-rPS-CTA macromonomers ($N_{sc} = 44$) and linear PS polymers ($N_m = 46$) at a 50:50 weight ratio. As the molecular weights of each constituent are approximately the same and both polymer chains are linear, any surface segregation will reflect enthalpic interactions. The outcomes of this test are presented in Figure S12. From the as-cast depth profile, we observe a slight enrichment of the NB-rPS-CTA macromonomers at the polymer-air interface. However, after annealing (2 days, 150 °C), there is a very slight depletion of the NB-rPS-CTA macromonomers from the interface, which supports the use of an attractive homopolymer-wall potential to describe interactions at the free surface.

The interactions in these blends are influenced by a range of system-specific attributes such as grafting density of side chains, monomer chemistry, chain-end chemistry, backbone chemistry and molecular weights. Therefore, the diagrams in Figure 3 and Figure 6, which summarize the types of surface segregation behaviors as a function of N_m/N_{sc} and N_b/N_{sc} , are not universal. To underline this point, Figure S19 shows depth profiles of comb copolymers with different grafting densities and a range of homopolymer-air interaction strengths. The values of N_m/N_{sc} that produce depletion, enrichment, or a condition of equal preference (“flat” profile) are changed in each case. However, the qualitative behaviors are similar for every combination of parameters that we model.

Conclusions

We report the surface segregation behaviors in thin film blends of linear polystyrene and 10 vol% bottlebrush polystyrene. We consider a broad parameter space that includes the degree

of polymerizations of linear polystyrene (N_m), bottlebrush backbone (N_b) and bottlebrush side chain (N_{sc}). Experiments based on time-of-flight secondary ion mass spectrometry reveal three types of behaviors at the film surface: enrichment of bottlebrush polymer, depletion of bottlebrush polymer, and equal preference for bottlebrush and linear polymers. These different behaviors are summarized in a simple schematic phase diagram as a function of N_b/N_{sc} and N_m/N_{sc} . Simulations based on the self-consistent field theory (SCFT) show that segregation behavior at a non-selective interface is governed by entropic effects and mainly depends on the ratio of N_m/N_{sc} . However, to reproduce the experimental findings, the SCFT model includes a weak enthalpic preference for the linear polymer towards the surface of the film. The origin of this enthalpic preference is not entirely clear, but the norbornene groups of the bottlebrush backbone may play a role. As these enthalpic interactions are system-specific, the schematic phase diagrams are not universal, but the general features should be observed with other bottlebrush/linear chemistries. Our study demonstrates that surface segregation behaviors are controlled by a combination of weak enthalpic and entropic driving forces. Notably, a concerted experimental and modeling effort can guide materials design and reduce experimental iteration, which is important for the development of coatings, films and adhesives based on architecturally-complex polymer blends.

Acknowledgement

The authors thank the National Science Foundation for financial support under award numbers CMMI-1727517 (A.H.M., T.S.L., G.E.S) and CMMI-1563008 and EEC-144950 (H.M., R.V.). Portions of the work-including the TOF-SIMS and the computations were conducted at the Center for Nanophase Materials Sciences, which is a US Department of Energy Office of Science User Facility.

Supporting Information. Synthesis of rPS macromonomers; NMR data; GPC data; AFM images; optical microscopy images; TOF-SIMS calibration; additional TOF-SIMS data;

spinodal for binary blends; supplemental simulations.

References

- (1) Koberstein, Jeffrey T., Molecular design of functional polymer surfaces. J. Polym. Sci., Part B: Polym. Phys. **2004**, 42, 2942–2956, DOI: 10.1002/polb.20157.
- (2) Narrainen, A. P.; Hutchings, L. R.; Ansari, I.; Thompson, R. L.; Clarke, N. Multi-End-Functionalized Polymers: Additives to Modify Polymer Properties at Surfaces and Interfaces. Macromolecules **2007**, 40, 1969–1980, DOI: 10.1021/ma062349y.
- (3) Pesek, S. L.; Lin, Y.-H.; Mah, H. Z.; Kasper, W.; Chen, B.; Rohde, B. J.; Robertson, M. L.; Stein, G. E.; Verduzco, R. Synthesis of bottlebrush copolymers based on poly(dimethylsiloxane) for surface active additives. Polymer **2016**, 98, 495–504, DOI: 10.1016/j.polymer.2016.01.057.
- (4) Hariharan, A.; Kumar, S. K.; Russell, T. P. A lattice model for the surface segregation of polymer chains due to molecular weight effects. Macromolecules **1990**, 23, 3584–3592, DOI: 10.1021/ma00217a009.
- (5) Hill, J. A.; Endres, K. J.; Mahmoudi, P.; Matsen, M. W.; Wesdemiotis, C.; Foster, M. D. Detection of Surface Enrichment Driven by Molecular Weight Disparity in Virtually Monodisperse Polymers. ACS Macro Lett. **2018**, 7, 487–492, DOI: 10.1021/acsmacrolett.7b00993.
- (6) Wu, D. T.; Fredrickson, G. H.; Carton, J.-P.; Ajdari, A.; Leibler, L. Distribution of chain ends at the surface of a polymer melt: Compensation effects and surface tension. J. Polym. Sci., Part B: Polym. Phys. **1995**, 33, 2373–2389, DOI: 10.1002/polb.1995.090331709.
- (7) Hariharan, A.; Kumar, S. K.; Russell, T. P. Free surfaces of polymer blends. I. Theoretical framework and application to symmetric polymer blends. J. Chem. Phys. **1993**, 98, 6516–6525, DOI: 10.1063/1.464792.

- (8) Walton, D. G.; Mayes, A. M. Entropically driven segregation in blends of branched and linear polymers. Phys. Rev. E **1996**, 54, 2811–2815, DOI: 10.1103/PhysRevE.54.2811.
- (9) Minnikanti, V. S.; Archer, L. A. Entropic Attraction of Polymers toward Surfaces and Its Relationship to Surface Tension. Macromolecules **2006**, 39, 7718–7728, DOI: 10.1021/ma061377d.
- (10) Qian, Z.; Minnikanti, V. S.; Sauer, B. B.; Dee, G. T.; Archer, L. A. Surface Tension of Symmetric Star Polymer Melts. Macromolecules **2008**, 41, 5007–5013, DOI: 10.1021/ma8002888.
- (11) Qian, Z.; Minnikanti, V. S.; Sauer, B. B.; Dee, G. T.; Kampert, W. G.; Archer, L. A. Surface tension of polystyrene blends: Theory and experiment. J. Polym. Sci., Part B: Polym. Phys. **2009**, 47, 1666–1685, DOI: 10.1002/polb.21771.
- (12) Minnikanti, V. S.; Archer, L. A. Surface migration of branched molecules: Analysis of energetic and entropic factors. J. Chem. Phys. **2005**, 123, 144902, DOI: 10.1063/1.2052627.
- (13) Minnikanti, V. S.; Archer, L. A. Surface enrichment of branched polymers in linear hosts: Effect of asymmetry in intersegmental interactions and density gradients. J. Chem. Phys. **2005**, 122, 084904, DOI: 10.1063/1.1850452.
- (14) Wu, D. T.; Fredrickson, G. H. Effect of Architecture in the Surface Segregation of Polymer Blends. Macromolecules **1996**, 29, 7919–7930, DOI: 10.1021/ma9602278.
- (15) Foster, M. D.; Greenberg, C. C.; Teale, D. M.; Turner, C. M.; Corona-Galvan, S.; Cloutet, E.; Butler, P. D.; Hammouda, B.; Quirk, R. P. Effective χ and surface segregation in blends of star and linear polystyrene. Macromol. Symp. **2000**, 149, 263–268, DOI: 10.1002/1521-3900(200001)149:1<263::AID-MASY263>3.0.CO;2-0.

- (16) Lee, J. S.; Lee, N.-H.; Peri, S.; Foster, M. D.; Majkrzak, C. F.; Hu, R.; Wu, D. T. Surface segregation driven by molecular architecture asymmetry in polymer blends. Phys. Rev. Lett. **2014**, 113, 225702, DOI: 10.1103/PhysRevLett.113.225702.
- (17) Fredrickson, G. H. Surfactant-induced lyotropic behavior of flexible polymer solutions. Macromolecules **1993**, 26, 2825–2831, DOI: 10.1021/ma00063a029.
- (18) Fredrickson, G. H.; Donley, J. P. Influence of broken conformational symmetry on the surface enrichment of polymer blends. J. Chem. Phys. **1992**, 97, 8941–8946, DOI: 10.1063/1.463969.
- (19) Fredrickson, G. H.; Liu, A. J.; Bates, F. S. Entropic Corrections to the Flory-Huggins Theory of Polymer Blends: Architectural and Conformational Effects. Macromolecules **1994**, 27, 2503–2511, DOI: 10.1021/ma00087a019.
- (20) Kumar, R.; Lokitz, B. S.; Sides, S. W.; Chen, J.; Heller, W. T.; Ankner, J. F.; Browning, J. F.; Kilbey II, S. M.; Sumpter, B. G. Microphase separation in thin films of lamellar forming polydisperse di-block copolymers. RSC Adv. **2015**, 5, 21336–21348, DOI: 10.1039/C5RA00974J.
- (21) Johnson, J. A.; Lu, Y. Y.; Burts, A. O.; Xia, Y.; Durrell, A. C.; Tirrell, D. A.; Grubbs, R. H. Drug-Loaded, Bivalent-Bottle-Brush Polymers by Graft-through ROMP. Macromolecules **2010**, 43, 10326–10335, DOI: 10.1021/ma1021506.
- (22) Zou, J.; Jafr, G.; Themistou, E.; Yap, Y.; Wintrob, Z. A. P.; Alexandridis, P.; Ceacareanu, A. C.; Cheng, C. pH-Sensitive brush polymer-drug conjugates by ring-opening metathesis copolymerization. Chem. Commun. **2011**, 47, 4493–4495, DOI: 10.1039/C0CC05531J.
- (23) Miyake, G. M.; Piunova, V. A.; Weitekamp, R. A.; Grubbs, R. H. Precisely Tunable Photonic Crystals From Rapidly Self-Assembling Brush Block Copolymer Blends. Angew. Chem. Int. Ed. **2012**, 51, 11246–11248, DOI: 10.1002/anie.201205743.

- (24) Kang, Y.; Walish, J. J.; Gorishnyy, T.; Thomas, E. L. Broad-wavelength-range chemically tunable block-copolymer photonic gels. Nat. Mater. **2007**, 6, 957–960, DOI: 10.1038/nmat2032.
- (25) Banquy, X.; Burdyńska, J.; Lee, D. W.; Matyjaszewski, K.; Israelachvili, J. Bioinspired Bottle-Brush Polymer Exhibits Low Friction and Amontons-like Behavior. J. Am. Chem. Soc. **2014**, 136, 6199–6202, DOI: 10.1021/ja501770y.
- (26) Faivre, J.; Shrestha, B. R.; Xie, G.; Delair, T.; David, L.; Matyjaszewski, K.; Banquy, X. Unraveling the Correlations between Conformation, Lubrication, and Chemical Stability of Bottlebrush Polymers at Interfaces. Biomacromolecules **2017**, 18, 4002–4010, DOI: 10.1021/acs.biomac.7b01063.
- (27) Li, X.; Prukop, S. L.; Biswal, S. L.; Verduzco, R. Surface Properties of Bottlebrush Polymer Thin Films. Macromolecules **2012**, 45, 7118–7127, DOI: 10.1021/ma301046n.
- (28) Walton, D. G.; Soo, P. P.; Mayes, A. M.; Sofia Allgor, S. J.; Fujii, J. T.; Griffith, L. G.; Ankner, J. F.; Kaiser, H.; Johansson, J.; Smith, G. D.; Barker, J. G.; Satija, S. K. Creation of Stable Poly(ethylene oxide) Surfaces on Poly(methyl methacrylate) Using Blends of Branched and Linear Polymers. Macromolecules **1997**, 30, 6947–6956, DOI: 10.1021/ma970698+.
- (29) Mitra, I.; Li, X.; Pesek, S. L.; Makarenko, B.; Lokitz, B. S.; Uhrig, D.; Ankner, J. F.; Verduzco, R.; Stein, G. E. Thin Film Phase Behavior of Bottlebrush/Linear Polymer Blends. Macromolecules **2014**, 47, 5269–5276, DOI: 10.1021/ma501070w.
- (30) Teng, C.-Y.; Sheng, Y.-J.; Tsao, H.-K. Boundary-induced segregation in nanoscale thin films of athermal polymer blends. Soft Matter **2016**, 12, 4603–4610, DOI: 10.1039/C6SM00559D.
- (31) Lee, J.; Quirk, R.; Foster, M. Effect of butadiene end-capping of arms in a star polystyrene on solution properties, bulk dynamics, and bulk thermody-

- namic interactions in binary blends. Macromolecules **2004**, 37, 10199–10204, DOI: 10.1021/ma048758g.
- (32) Lee, J. S.; Foster, M. D.; Wu, D. T. Effects of branch points and chain ends on the thermodynamic interaction parameter in binary blends of regularly branched and linear polymers. Macromolecules **2006**, 39, 5113–5121, DOI: 10.1021/ma060023j.
- (33) Jones, R. A. L.; Kramer, E. J.; Rafailovich, M. H.; Sokolov, J.; Schwarz, S. A. Surface Enrichment in an Isotopic Polymer Blend. Phys. Rev. Lett. **1989**, 62, 280–283, DOI: 10.1103/PhysRevLett.62.280.
- (34) Li, Z.; Zhang, K.; Ma, J.; Cheng, C.; Wooley, K. L. Facile syntheses of cylindrical molecular brushes by a sequential RAFT and ROMP ‘grafting-through’ methodology. J. Polym. Sci., Part A: Polym. Chem. **2009**, 47, 5557–5563, DOI: 10.1002/pola.23626.
- (35) Sanford, M. S.; Love, J. A.; Grubbs, R. H. A Versatile Precursor for the Synthesis of New Ruthenium Olefin Metathesis Catalysts. Organometallics **2001**, 20, 5314–5318, DOI: 10.1021/om010599r.
- (36) Stafford, C. M.; Roskov, K. E.; Epps, T. H.; Fasolka, M. J. Generating thickness gradients of thin polymer films via flow coating. Rev. Sci. Instrum. **2006**, 77, 023908, DOI: 10.1063/1.2173072.
- (37) Macfarlane, R. J.; Kim, B.; Lee, B.; Weitekamp, R. A.; Bates, C. M.; Lee, S. F.; Chang, A. B.; Delaney, K. T.; Fredrickson, G. H.; Atwater, H. A.; Grubbs, R. H. Improving Brush Polymer Infrared One-Dimensional Photonic Crystals via Linear Polymer Additives. J. Am. Chem. Soc. **2014**, 136, 17374–17377, DOI: 10.1021/ja5093562, PMID: 25373000.
- (38) Dalsin, S. J.; Rions-Maehren, T. G.; Beam, M. D.; Bates, F. S.; Hillmyer, M. A.; Matsen, M. W. Bottlebrush Block Polymers: Quantitative Theory and Experiments. ACS Nano **2015**, 9, 12233–12245, DOI: 10.1021/acsnano.5b05473, PMID: 26544636.

- (39) Bates, F. S.; Wignall, G. D. Isotope-induced quantum-phase transitions in the liquid state. Phys. Rev. Lett. **1986**, 57, 1429.
- (40) Matsen, M. W. Thin Films of Block Copolymer. J. Chem. Phys. **1997**, 106, 7781–7791.
- (41) Takahashi, H.; Laachi, N.; Delaney, K. T.; Hur, S.-M.; Weinheimer, C. J.; Shykind, D.; Fredrickson, G. H. Defectivity in Laterally Confined Lamella-Forming Diblock Copolymers: Thermodynamic and Kinetic Aspects. Macromolecules **2012**, 45, 6253–6265.
- (42) Fredrickson, G. H. The Equilibrium Theory of Inhomogeneous Polymers; Oxford University Press: New York, 2006.
- (43) <https://www.txcorp.com>.
- (44) Cummings, J.; Lowengrub, J. S.; Sumpter, B. G.; Wise, S. M.; Kumar, R. Modeling solvent evaporation during thin film formation in phase separating polymer mixtures. Soft Matter **2018**, 14, 1833–1846, DOI: 10.1039/C7SM02560B.
- (45) Cheng, S.; Grest, G. S. Dispersing Nanoparticles in a Polymer Film via Solvent Evaporation. ACS Macro Lett. **2016**, 5, 694–698, DOI: 10.1021/acsmacrolett.6b00263.
- (46) Kawaguchi, D.; Tanaka, K.; Torikai, N.; Takahara, A.; Kajiyama, T. Surface and Interfacial Segregation in Blends of Polystyrene with Functional End Groups and Deuterated Polystyrene. Langmuir **2007**, 23, 7269–7275, DOI: 10.1021/1a700418j.

Graphical TOC Entry

